Lung Tissue Analysis Using Isotropic Polyharmonic B–Spline Wavelets

Adrien Depeursinge[1], Dimitri Van De Ville[2], Michael Unser[2], and Henning Müller[1,3]

[1] Service of Medical Informatics, Geneva University Hospitals and University of Geneva, CH, adrien.depeursinge@sim.hcuge.ch,
[2] Biomedical Imaging Group, École Polytechnique Fédérale de Lausanne, CH,
[3] Business Information Systems, University of Applied Sciences Sierre, CH.

Abstract. A texture classification system is described, based on isotropic polyharmonic B–spline wavelets that identify lung tissue patterns from high–resolution computed tomography (HRCT) images of patients affected with interstitial lung diseases (ILD). Along with several desirable properties for isotropic texture analysis, the nonseparable transform with a quincunx subsambling scheme allows a mean of 94.3% of correct matches among six lung tissue classes. A comparison with a classical dyadic transform suggests that the isotropic quincunx transform is preferable for lung tissue analysis. This is part of work on a tool for integrating visual and clinical features as diagnostic aid for emergency radiology.

1 Introduction

The interpretation of high–resolution computed tomography (HRCT) images of the chest showing patterns associated with interstitial lung diseases (ILDs) is time–consuming and requires high clinical expertise due to rare cases and a large number of different diseases. The diagnosis of ILD is established from the interpretation of several clinical parameters of the patient in addition to radiological findings [1]. The most common imaging procedure used is the chest x–ray because of its low cost and weak radiation exposure. However, chest x–rays appear as normal in a large portion of diseases and are often unspecific where HRCT of the chest contains essential visual data for the characterization of lung tissue patterns associated with ILDs [2]. HRCT produces three–dimensional (3D) images of the pulmonary volumes, avoids the superposition of anatomic structures, and is well suited for the assessment of lung tissue texture. However, the increase of data volume compared to the chest x–rays makes the interpretation task more complex. The high spatial resolution generates a large variety of lung tissue patterns, which induces confusion of diverse pathologic lung tissues. In addition, the radiologist has to go through the whole stack of slices, which can result in interpretation errors by omission [3]. In emergency radiology, radiologists have recourse to a large diversity of imaging modalities such as conventional

projection radiography, computed tomography (CT), magnetic resonance imaging (MRI), functional imaging (fMRI, PET), and ultrasound applied to different organs such as the brain, colon, breast, chest, liver, kidney and the vascular and skeletal systems. They have to provide a first radiological report with ideas on the diagnosis quickly. Automatic detection and categorization of pathologic lung tissue patterns can help the radiologists to cope with the complexity and challenges of interpreting HRCT [4, 5]. The suspicious (abnormal) patterns in the new, non–interpreted HRCT are highlighted to the radiologist with a proposed tentative diagnostic [6]. The radiologist has to consider the system as a second opinion for providing a differential diagnosis.

The taxonomy used by radiologists to interpret patterns in HRCT images often relates to texture properties, which suggest that texture analysis is relevant for the characterization of ILD which is typically diffuse. Texture analysis in digital image processing has been an active research domain over more than thirty years. In [7], texture in digital images is defined as nonfigurative and cellularly organized areas of pixels. Early examples of texture features are the autocorrelation function, textural edginess, measurements derived from mathematical morphology, run–length and gray–level co–occurence matrices, the latter being the most popular of the lot [7, 8]. Unfortunately, building co–occurence matrices from HRCT images where grey–levels are corresponding to Hounsfield Units (H.U.) with values from –1000 H.U. (air) to 1500 H.U. (high density bones) is unrealistic because the number of possible co-occurrences is simply too large to be stored and estimated reliably. Complementary to the characterization of spatial dependencies, the distribution of grey–levels values can be studied through statistical measures of grey–level histograms. The Fourier transform has also been proposed for texture analysis, based on the property that some image patterns (especially, periodic ones) are well described in terms of sinusoidal components [8, 9]. However, the latter is not appropriate for segmentation because the Fourier transform is global.

1.1 Dyadic Versus Quincunx Wavelet Frames for Texture Analysis

The multiresolution analysis provided by the wavelet transform (WT) is an attractive solution for texture analysis. The signal under investigation is decomposed onto a set of wavelet functions at various scales; i.e., representing details at different resolutions. For example, in the discrete version with dyadic subsampling the analyzed image is iteratively filtered and subsampled by a factor of 2 in each dimension. The WT is particularly well suited to compactly represent piecewise–smooth signals, which partly explains its success in biomedical imaging applications [10]. Wavelet bases are desirable to perform compact data representations, as they allow orthogonal decompositions. They have fast implementations, but have the main drawback to lack translation invariance. Discrete wavelet frames (DWF), on the other hand, are redundant and offer more flexibility for image analysis. DWF are truly shift–invariant and can be obtained from a wavelet basis by removing the subsampling stage of the algorithm and upsampling the filters instead. When compared to the WT, the DWF tends to decrease

the variability of the estimated texture features thereby improving classification performance [11].

Although widely deployed, the separable dyadic form of DWF has two major drawbacks to perform texture analysis. On one hand, the scale–progression is large as images are downsampled by a factor of 2 (in each dimension) between two decomposition levels. Relevant information might be padded out when having major energy contained in a narrow subband located between two successive levels of the dyadic transform. Subtle changes in the scale of lung tissue patterns (i.e. micronodules versus macronodules) might be neglected by the dyadic scale–progression [12]. On the other hand, separability allows computational efficiency because wavelet coefficients within each subband can be obtained by successive one–dimensional (1D) convolutions along the columns and the rows of the image. Unfortunately, this process tends to favor the vertical and the horizontal directions, and produces a so–called "diagonal" wavelet component, which does not have a straightforward directional interpretation. Under the assumption that lung tissue patterns in axial slices of HRCT data do not have privileged directionalities, neither horizontal, vertical, nor diagonal, the separable transform is not appropriate for their analysis.

In Section 2.2, we propose the use of isotropic polyharmonic B–spline wavelets together with a fine scale–progression (equivalent factor of $\sqrt{2}$ based on the quincunx subsampling scheme). Beside scale–progression and isotropy we demonstrate that isotropic polyharmonic B–splines have many other desirable properties for lung tissue analysis.

1.2 Non–Separable Wavelets for Biomedical Texture Classification

During the last twenty years, the WT has been utilized widely in biomedical applications, as well as for the characterization of textures of biomedical tissues [10]. The increased spatial resolution of modern imaging techniques allows for assessment from anatomical structures to textures of tissues. More recently, nonseparable wavelet transforms have been used for detection of pathologic tissues with no a priori privileged directionalities in several imaging modalities.

In [13], the quincunx wavelet transform is used for the characterization of liver tissue in noisy ultrasonic B–scan images. Compared to the classical WT, the nonseparable transform allows for an increased classification performance. However, the use of the compacted pyramidal representation of the subbands is not appropriate to obtain shift–invariant features for classification.

The redundant quincunx wavelet transform along with support vector machines (SVM) were used in [14] to classify 5 lung tissue patterns associated with ILDs and achieved 94.3% of global accuracy. Nevertheless, the classification task is slightly biased since the training set contains an equal number of instances for each of the five patterns, which is usually not the case in clinical practice.

In [12], grey–level histograms with discrete wavelet frame features were evaluated using a k–nearest neighbor classifier. In this paper, we use isotropic polyharmonic B–splines as scaling functions to implement a two–dimensional (2D) redundant quincunx wavelet transform in order to characterize 6 types of lung

tissue in HRCT data with optimized SVMs. Lung tissue texture classification using co-occurence matrices, Gabor filters and Tamura texture features was investigated in [15]. The classification of regions of interest (ROIs) delineated by the user consitutes the intial steps towards automatic detection of abnormal lung tissue patterns in the whole HRCT volume.

2 Methods

2.1 Dataset

The dataset used is part of an internal multimedia database of ILD cases containing HRCT images with annotated ROIs created in the *Talisman* project[1]. 843 ROIs from healthy and five pathologic lung tissue patterns are selected for training and testing the classifiers selecting classes with sufficiently high representation (see Table 1).

The wavelet frame decompositions with dyadic and quincunx subsampling are implemented in Java [11, 16] as well as optimization of SVMs. The basic implementation of the SVMs is taken from the open source Java library *Weka*[2].

Table 1. Visual aspect and distribution of the ROIs per class of lung tissue pattern.

visual aspect	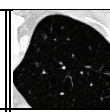	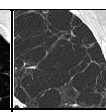	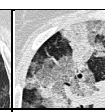	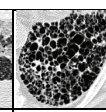	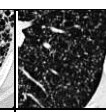	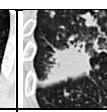
class	healthy	emphysema	ground glass	fibrosis	micronodules	macronodules
# of ROIs	113	93	148	312	155	22
# of patients	11	6	14	28	5	5

2.2 Isotropic Polyharmonic B–Spline Wavelets

As mentioned in Section 1.1, isotropic analysis is preferable for lung texture characterization. The Laplacian operator plays an important role in image processing and is clearly isotropic. Indeed, $\Delta = \frac{\partial^2}{\partial x_1^2} + \frac{\partial^2}{\partial x_2^2}$, is rotationally invariant. The polyharmonic B–spline wavelets implement a multiscale smoothed version of the Laplacian [16]. This wavelet, at the first decomposition level, can be characterized as

$$\psi_\gamma(\mathbf{D}^{-1}\mathbf{x}) = \Delta^{\frac{\gamma}{2}}\{\phi\}(\mathbf{x}), \tag{1}$$

[1] TALISMAN: Texture Analysis of Lung ImageS for Medical diagnostic AssistaNce, http://www.sim.hcuge.ch/medgift/01_Talisman_EN.htm

[2] http://www.cs.waikato.ac.nz/ml/weka/

where ϕ is an appropriate smoothing (low–pass) function and $\mathbf{D} = [1\ 1; 1\ -1]$ is the quincunx subsampling matrix. The so-called *order* γ tunes the iterate of the Laplacian operator (comparable to the traditional vanishing moments). Large values of γ reduce the energy of the wavelet coefficients but increase the ringing effect [17].

2.3 Lung Tissue Classification: Dyadic Versus Quincunx

The quincunx scale–progression is finer compared to dyadic decomposition, with an equivalent downsampling factor of $\sqrt{2}$ instead of 2. Compared to the dyadic separable case, quincunx subsampling generates only one wavelet subband per decomposition level (versus three for dyadic). This leads to a direct and easy interpretation of the subbands; the small number of subbands also breeds small features spaces, which are preferable for classification.

In summary, using isotropic polyharmonic B–splines as scaling functions have the following desirable properties for lung tissue analysis:

- rotational invariance
- fine scale progression tunable through γ
- easy and direct interpretation (one wavelet subband per scale)

2.4 Feature space

In order to build the feature space for further classification of the ROIs, several measures are computed from the original image as well as from the wavelet coefficients of each subband. On the original images, values of pixels belonging to the ROIs are categorized into 22 bins of grey–level histograms of Hounsfield Units (H.U.) in $[-1050; 600[$. The distributions of the wavelet coefficients in each subband are characterized through the parameters of mixtures of two Gaussians, which have shown to characterize distributions of wavelet coefficients well in [18]. With fixed means $\mu_{1,2} = \mu$, the standard–deviations $\sigma_{1,2}$ are estimated using the expectation–maximization (EM) algorithm. Under the assumption that the global mean of the coefficient values is close to zero (according to the admissibility conditions of wavelets), using two standard–deviations allows a reasonable fit of the distributions (see Figure 1). The feature vector thus consists of 24 features for 8 levels of the quincunx transform. Features are extracted for orders $\gamma = 2, 3, 4$. To compare performances, 4 levels of the classical dyadic transform (using frames as well) were performed using B–Spline wavelets of degree $\alpha = 1, 2, 3$. Indeed, the equivalent order of derivatives γ corresponds to $\alpha + 1$. Using parameters of a mixture of two Gaussians for each subband, the feature vector contains 36 measures of the dyadic wavelet frames coefficients (more details can be found in [12]).

3 Results

Feature vectors from 843 ROIs containing healthy and five pathologic lung tissues are extracted. 674 instances (80%) are randomly drawn from the full dataset and

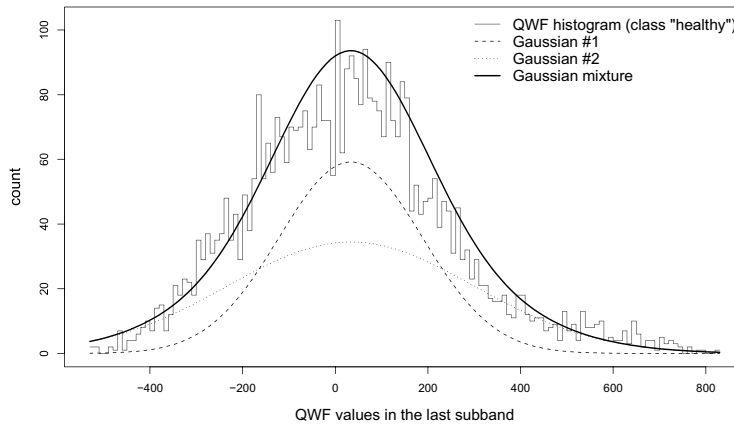

Fig. 1. Mixture of two Gaussians ($\mu_{1,2} = \mu$, $\sigma_{1,2}$) to modelize the distribution of wavelet coefficients within one subband.

used to train and optimize the parameters of Support Vector Machines (SVMs) with Gaussian kernel, which have shown to be effective to categorize texture in wavelet feature spaces in [19] and in particular lung tissue in [20]. The remaining 169 instances are used for testing. The global experimentation is repeated 30 times and means of the global classification accuracies along with means of class–specific accuracies are computed. A detailed description of the selection of the parameters of SVMs and a comparison of 5 common implementations of classifiers families can be found in [20]. Pairwise comparisons of classification accuracies using dyadic versus quincunx wavelet frames for several orders $(\alpha+1, \gamma)$ are shown in Table 2.

4 Discussion

Pairwise comparisons shown in Table 2 indicate that quincunx wavelets outperform dyadic ones in 91.7% of the comparisons (22 among 24). This global increase in performance is primarily due to the better isotropy properties of these non-separable wavelets, which is due to their close connection to the Laplacian. Indeed, the favored directions of the separable transform lead to noisy features breeding non–homogeneous clusters of instances belonging to the same class in the feature space, which decreases global classification performance. Although having influence on global accuracy as well, the finer scale progression allowed by the quincunx subsampling scheme increases the precision of the classification;

Table 2. Mean accuracies in % with experiments repeated 30 times. Isotropic polyharmonic B–spline wavelets with order $\gamma = 3$ allowed a mean of 94.3% of correct predictions among the six lung tissue classes with high precision (geometric mean = 89%).

class		$\alpha = 1, \gamma = 2$	$\alpha = 2, \gamma = 3$	$\alpha = 3, \gamma = 4$
healthy	dyadic	91.1	93.6	92.5
	quincunx	95.9	98.1	92.4
emphysema	dyadic	97.2	98.7	97.7
	quincunx	100	100	99.7
ground glass	dyadic	84.2	88.3	86.3
	quincunx	85.7	89	87.7
fibrosis	dyadic	95.8	95.2	96.5
	quincunx	96.5	96.3	94.5
micronodules	dyadic	89.8	93.3	88.8
	quincunx	94.1	95.2	91.7
macronodules	dyadic	40.3	48	46.9
	quincunx	54.2	55.5	48.5
geometric mean	dyadic	83.1	86.2	84.8
	quincunx	87.8	89	85.7
global mean	dyadic	90.6 ± 2.6	92.5 ± 1.4	91.4 ± 2.2
	quincunx	93.3 ± 1.6	$\mathbf{94.3 \pm 1.6}$	92 ± 1.9

i.e., by avoiding confusion between patterns with well–defined object sizes, such as *micro–* and *macro– nodules*.

Global accuracy values are trustworthy for further usage in clinical routine as the six classes of lung tissue pattern tested allow for diagnosing a wide variety of ILDs [2]. Compared to other studies on lung tissue analysis in HRCT data, our system is closer to clinical routine as the distributions of the classes are realistic contrary to [14] and we include healthy tissue (which is not the case in [4]). Indeed, healthy tissue is the most difficult to separate from others as the variety is by far the largest.

5 Conclusion

The ability of dyadic versus quincunx wavelet transforms to analyze lung tissue in HRCT data were evaluated on a high–quality dataset. Isotropic polyharmonic B–spline wavelets with optimized order allowed a mean of 94.3% correct predictions among six lung tissue classes associated with ILDs with high precision. Pairwise comparisons with a dyadic transform showed that the polyharmonic wavelets outperforms the classical separable frames 22 times among 24, which suggest that the latter is more appropriate for lung tissue analysis in HRCT data.

Further work has to be carried out in order to integrate clinical parameters for classifying the lung tissue regions, in the same way the radiologists interpret HRCT images. First experiments showed high potential for improving classification performances in [21].

6 Acknowledgments

This work was supported by the Swiss National Science Foundation (FNS) with grant 200020–118638/1 and the equalization fund of Geneva University Hospitals and University of Geneva (grant 05–9–II) and the EU 6^{th} Framework Program in the context of the KnowARC project (IST 032691).

References

1. Flaherty, K.R., King, T.E., Ganesh Raghu, J., Lynch III, J.P., Colby, T.V., Travis, W.D., Gross, B.H., Kazerooni, E.A., Toews, G.B., Long, Q., Murray, S., Lama, V.N., Gay, S.E., Martinez, F.J.: Idiopathic interstitial pneumonia: What is the effect of a multidisciplinary approach to diagnosis? American Journal of Respiratory and Critical Care Medicine **170** (July 2004) 904–910
2. Stark, P.: High resolution computed tomography of the lungs. UpToDate **September** (2007)
3. Kakinuma, R., Ohmatsu, H., Kaneko, M., Eguchi, K., Naruke, T., Nagai, K., Nishiwaki, Y., Suzuki, A., Moriyama, N.: Detection failures in spiral CT screening for lung cancer: Analysis of CT findings. Radiology **212** (July 1999) 61–66
4. Shyu, C.R., Brodley, C.E., Kak, A.C., Kosaka, A., Aisen, A.M., Broderick, L.S.: ASSERT: A physician–in–the–loop content–based retrieval system for HRCT image databases. Computer Vision and Image Understanding (special issue on content–based access for image and video libraries) **75**(1/2) (July/August 1999) 111–132
5. Müller, H., Michoux, N., Bandon, D., Geissbuhler, A.: A review of content–based image retrieval systems in medicine – clinical benefits and future directions. International Journal of Medical Informatics **73** (February 2004) 1–23
6. Sinha, U., Bui, A., Taira, R., Dionisio, J., Morioka, C., Johnson, D., Kangarloo, H.: A review of medical imaging informatics. Annals of the New York Acedemy of Sciences **980** (December 2002) 168–197
7. Haralick, R.M.: Statistical and structural approaches to texture. Proceedings of the IEEE **67**(5) (May 1979) 786–804
8. Reed, T.R., du Buf, J.M.H.: A review of recent texture segmentation and feature extraction techniques. Computer Vision, Graphics and Image Processing **57**(3) (May 1993) 359–372
9. Hsu, T.I., Calway, A.D., Wilson, R.: Texture analysis using the multiresolution fourier transform. In: Proc 8th Scandinavian Conference on Image Analysis, IAPR (May 1993) 823–830
10. Unser, M., Aldroubi, A.: A review of wavelets in biomedical applications. Proceedings of the IEEE **84**(4) (April 1996) 626–638
11. Unser, M.: Texture classification and segmentation using wavelet frames. IEEE Transactions on Image Processing **4**(11) (1995) 1549–1560
12. Depeursinge, A., Sage, D., Hidki, A., Platon, A., Poletti, P.A., Unser, M., Muller, H.: Lung tissue classification using wavelet frames. Engineering in Medicine and Biology Society, 2007. EMBS 2007. 29th Annual International Conference of the IEEE (August 2007) 6259–6262
13. Mojsilovic, A., Popovic, M., Markovic, S., Krstic, M.: Characterization of visually similar diffuse disease from b-scan liver images using nonseparable wavelet transform. IEEE Trans. Med. Imaging **17**(4) (August 1998) 541–549

14. Shamsheyeva, A., Sowmya, A.: The anisotropic gaussian kernel for SVM classification of HRCT images of the lung. In: Proceedings of the 2004 Intelligent Sensors, Sensor Networks and Information Processing Conference. (December 2004) 439–444
15. Müller, H., Marquis, S., Cohen, G., Geissbuhler, A.: Lung CT analysis and retrieval as a diagnostic aid. In: Medical Informatics Europe (MIE 2005), Geneva, Switzerland (August 2005) 453–458
16. Van De Ville, D., Blu, T., Unser, M.: Isotropic polyharmonic B-Splines: Scaling functions and wavelets. IEEE Transactions on Image Processing **14**(11) (November 2005) 1798–1813
17. Feilner, M., Van De Ville, D., Unser, M.: An orthogonal family of quincunx wavelets with continuously adjustable order. IEEE Transactions on Image Processing **14**(4) (April 2005) 499–510
18. Portilla, J., Strela, V., Wainwright, M.J., Simoncelli, E.P.: Image denoising using scale mixtures of gaussians in the wavelet domain. IEEE Transactions on Image Processing **12**(11) (November 2003) 1338–1351
19. Li, S., Kwok, J.T., Zhu, H., Wang, Y.: Texture classification using the support vector machines. Pattern Recognition **36**(12) (December 2003) 2883–2893
20. Depeursinge, A., Iavindrasana, J., Hidki, A., Cohen, G., Geissbuhler, A., Platon, A., Poletti, P.A., Müller, H.: A classification framework for lung tissue categorization. In Andriole, K.P., Siddiqui, K.M., eds.: Medical Imaging 2008: PACS and Imaging Informatics. Volume 6919., SPIE (April 2008) 69190C
21. Depeursinge, A., Iavindrasana, J., Cohen, G., Platon, A., Poletti, P.A., Müller, H.: Lung tissue classification in HRCT data integrating the clinical context. In: 2008 21st IEEE International Symposium on Computer-Based Medical Systems, Jyväskylä, Finland (June 2008) 542–547